ACES Asian Chemical Editorial Society

DOI: 10.1002/cnma.201700076

CHEMNANOMAT
Full Paper

Electrocatalysis

# Electrocatalysis of Furfural Oxidation Coupled with $H_2$ Evolution via Nickel-Based Electrocatalysts in Water

Nan Jiang[+],[a] Xin Liu[+],[a, b] Jinmei Dong,[b] Bo You,[a] Xuan Liu,[a] and Yujie Sun*[a]

**Abstract:** Electrocatalytic water splitting has been widely considered as a promising approach to produce clean $H_2$. The anodic half reaction of water splitting, the $O_2$ evolution reaction (OER), is the kinetic bottleneck of the overall process and its product $O_2$ is not of high value. Herein, we report a novel strategy to replace OER with a thermodynamically more favorable anodic reaction, furfural oxidation to 2-furoic acid. Furfural is one of the dehydration products of biomass and its oxidation product 2-furoic acid has many industrial applications. A bifunctional electrocatalyst of $Ni_2P$-derived arrays on nickel foam ($Ni_2P$/Ni/NF) was developed for the integrated electrocatalysis of both furfural oxidation and $H_2$ production. When $Ni_2P$/Ni/NF acts as the electrocatalyst for both anode and cathode, nearly 100% Faradaic efficiencies for $H_2$ evolution and furfural oxidation were obtained. Such an integrated electrolysis catalyzed by $Ni_2P$/Ni/NF required an applied voltage $\approx$110 mV smaller than that of pure water splitting to achieve the current density of 10 mA cm$^{-2}$, together with robust stability. Overall, our novel electrolyzer produced valuable products at both electrodes ($H_2$ at cathode and 2-furoic acid at anode) and may extend to the coupling of $H_2$ evolution with many other valuable organic oxidation reactions.

## Introduction

Rapid growth of global energy demands, declining fossil fuel reserves, and climate change resulting from the utilization of fossil fuels collectively drive the academic interest to explore renewable and clean energy resources.[1] As such, electrochemical or photoelectrochemical water splitting with renewable energy input, such as solar and wind, to produce $H_2$ and $O_2$ has been widely recognized as a promising approach to meet future energy needs with minimal environmental impact.[2] However, the oxidative half reaction of water splitting, the $O_2$ evolution reaction (OER), is always the bottleneck of the overall water splitting process because of its more sluggish kinetics;[3] while the product of OER, $O_2$, is not a chemical of high market value. On the other hand, even though $H_2$ is a great energy carrier (and fuel) produced from water splitting, there are no carbon-based organic compounds that could be derived from water splitting electrocatalysis. In fact, fossil materials still play the dominant role in producing organic chemicals. Therefore, it will be highly desirable to replace OER with alternative organic oxidation reactions which are not only more thermodynamically favorable than OER but also produce carbon-based products of significant value. Under this scenario, two types of value-added products (i.e., $H_2$ and upgraded organic compound) will be yielded at both the cathode and anode of an electrolyzer, maximizing the return of voltage input.

In order to realize a green and carbon-neutral economy, biomass refining has attracted increasing attention these years, as biomass is the largest natural source of carbon whose utilization will not alter the carbon balance of the current ecosystem because biomass stores contemporary carbon.[4] Derived from the hydrolysis/dehydration of carbohydrates such as corncobs and bagasse,[5] furfural is widely regarded as a versatile platform biomass intermediate, because it can be converted to many highly valuable chemical feedstocks.[6] For instance, furfural can be reduced to furfuryl alcohol, furan, cyclopentanone, cyclopentanol, and tetrahydrofurfuryl alcohol, etc., most of which can act as biofuels or building blocks for the synthesis of fine chemicals.[7] On the other hand, its oxidation product, 2-furoic acid, is an excellent feedstock in organic synthesis and an important intermediate in the production of medicines and perfumes.[8] Meanwhile, 2-furoic acid can also work as a starting material for the production of furoate esters.[9] As a result, many efforts have been devoted to exploring the conversion of furfural into 2-furoic acid recently. Most previous studies of oxidation of furfural into 2-furoic acid have been investigated in traditional heterogeneous systems under aerobic conditions

[a] N. Jiang,[+] Dr. X. Liu,[+] Dr. B. You, X. Liu, Dr. Y. Sun
Department of Chemistry and Biochemistry
Utah State University
0300 Old Main Hill, Logan, Utah 84322 (USA)
E-mail: yujie.sun@usu.edu

[b] Dr. X. Liu,[+] Dr. J. Dong
Key Laboratory of Comprehensive and Highly Efficient Utilization of Salt Lake Resources
Chinese Academy of Sciences
18 Xinning Road, Xi'ning 810008 (China)

[+] These authors contributed equally to this work.

Supporting information and the ORCID identification number(s) for the author(s) of this article can be found under https://doi.org/10.1002/cnma.201700076.

with noble metal catalysts (Pt, Au, and Pd).[10] Under certain conditions, the conversion even needs strong chemical oxidants rather than $O_2$.[11] These high-cost and energy-demanding strategies prompted us to develop alternative approaches for furfural oxidation. Electrocatalytic oxidation of furfural in which the oxidation is driven by electricity is a promising approach (Scheme 1).

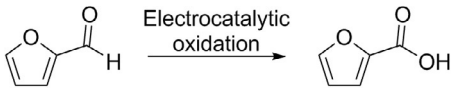


**Scheme 1.** Oxidation of furfural to 2-furoic acid.

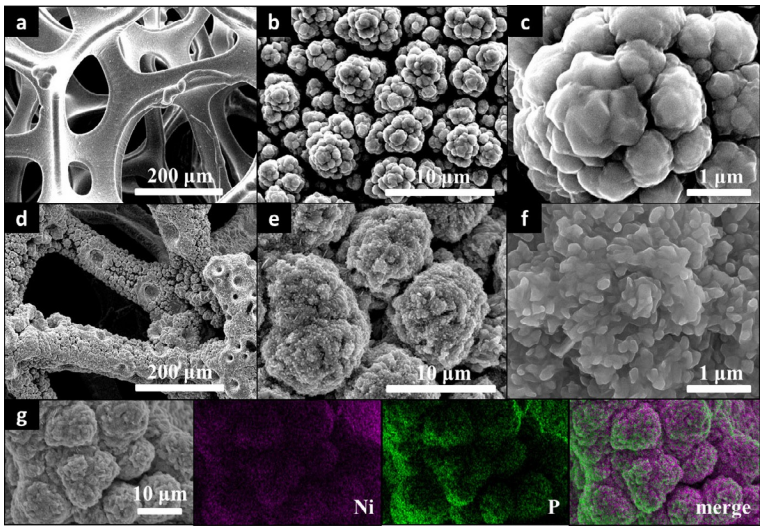


**Figure 1.** SEM images of (a) NF, (b, c) Ni/NF at different magnifications, (d–f) $Ni_2P$/Ni/NF at different magnifications, and (g) the elemental mapping images of $Ni_2P$/Ni/NF showing the distributions of Ni and P.

Our group and others have been interested in developing inexpensive electrocatalytic systems strategies for water splitting[12] and biomass upgrading,[13] such as the oxidation of 5-hydroxymethylfurfural (HMF) to 2,5-furandicarboxylic acid. The two functional groups (alcohol and aldehyde) in HMF complicate the mechanistic understanding of its oxidation process. In this regard, furfural with only an aldehyde for oxidation can act as perfect control candidate to be investigated. In addition, the oxidation of furfural is an important reaction by itself, as mentioned above. In the present study, we demonstrate that a low-cost bifunctional nickel-based electrocatalyst is able to catalyze both $H_2$ production and furfural oxidation to 2-furoic acid in alkaline electrolyte. A nearly complete furfural conversion and 98% yield of 2-furoic acid were obtained at the anode under ambient conditions. Similarly, efficient $H_2$ production was achieved at the cathode with nearly unity Faradaic efficiency and long-term stability. When a two-electrode electrolyzer was constructed with the nickel-based electrocatalysts acting as both cathode and anode electrocatalysts, integrated generation of $H_2$ and 2-furoic acid was realized simultaneously with nearly 100% Faradaic efficiency and robust stability for both half reactions.

## Results and Discussion

$Ni_2P$/Ni/NF was prepared according to our published method (see the Experimental Section for details).[14] The commercially available nickel foam has a porous structure with smooth skeleton as shown in Figure 1a. After electrodeposition of nickel, fine nickel particles (diameter of 0.5–1 μm) were grown on the nickel foam (Ni/NF, Figure 1b–c), in sharp contrast to the smooth surface of the pristine nickel foam (Figure 1a). Upon low-temperature phosphidation, the metallic Ni transformed to $Ni_2P$ (Figure 1d–f), which could be confirmed by their XRD patterns (Figure S1 in the Supporting Information). The corresponding elemental mapping images of Ni and P in $Ni_2P$/Ni/NF demonstrated the uniform distribution of Ni and P throughout the whole sample (Figure 1g), in agreement with the successful conversion from Ni/NF to $Ni_2P$/Ni/NF post phosphidation. X-ray photoelectron spectroscopy (XPS) was conducted to probe the composition of $Ni_2P$/Ni/NF and the valence state of each element. The XPS survey spectrum shown in Figure S2 exhibits all the anticipated elements including Ni and P. The high-resolution Ni 2p XPS spectrum shown in Figure S3a could be deconvoluted to peaks at 853.2, 855.6, and 860.9 eV, which were assigned to Ni $\delta^+$ in $Ni_2P$, oxidized Ni species, and the Ni $2p_{3/2}$ satellite peak of $Ni_2P$, respectively.[15] The deconvolution of the high-resolution P 2p XPS spectrum (Figure S3b) led to a prominent peak in the region of 129–130 eV, which could be attributed to the phosphide signal. The other peak around 134.4 eV was due to the oxidized phosphorus species on surface because of exposure to air prior to the XPS measurement. Overall, Ni has partial positive charge ($\delta^+$) while P shows partial negative charge ($\delta^-$) in $Ni_2P$/Ni/NF, indicative of the transfer of electron density from Ni to P, which is consistent with previous reports.[14]

Since $Ni_2P$ has been well-demonstrated to be an effective electrocatalyst for $H_2$ evolution in water,[14] herein we were more interested in exploring whether it was able to catalyze the furfural oxidation in alkaline electrolyte (1.0 M KOH). All the electrochemical experiments were conducted in a three-electrode configuration with a two-compartment cell separated by an anion-exchange membrane, unless otherwise noted. For most organic oxidation reactions in water, it is well-known that $O_2$ evolution could potentially be the competing reaction.[16] Therefore, it is important to check the oxidation current in the absence of organic substrates. As shown in Figure 2a, the cyclic voltammogram of $Ni_2P$/Ni/NF in 1.0 M KOH exhibited a catalytic oxidation current at an onset of 1.55 V vs. RHE (reversible hydrogen electrode). In order to avoid the interference of the redox feature of the nickel catalyst itself, only cathodic scan of the cyclic voltammogram was plotted in Figure 2a.[17] Further scanning towards more positive potential produced a dramatic increase in current density accompanied with vigorous $O_2$ bubble formation on the electrode surface. Upon the addition of 30 mM furfural, a catalytic current was observed at

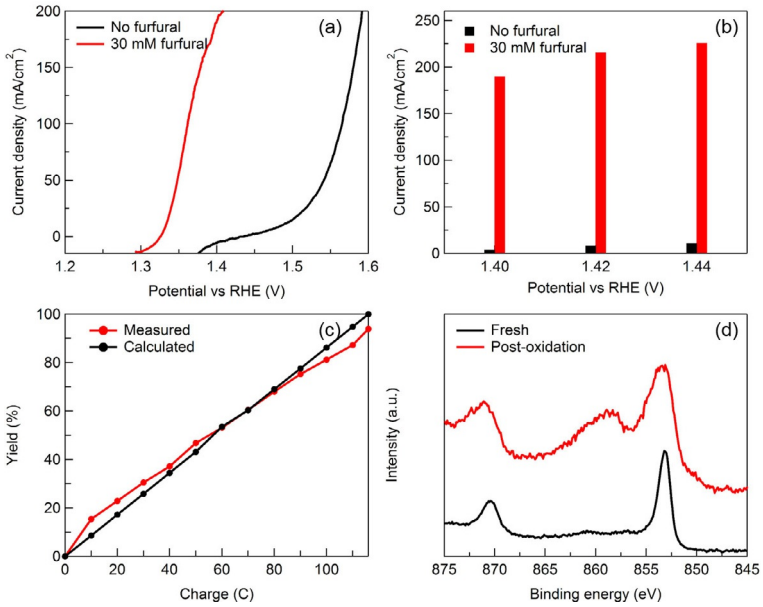


**Figure 2.** (a) The cathodic scans of cyclic voltammograms of $Ni_2P$/Ni/NF with (red) and without (black) 30 mM furfural at a scan rate of 2 mV s$^{-1}$ in 1.0 M KOH. (b) Comparison of the current density of $Ni_2P$/Ni/NF and NF at 1.40, 1.42, and 1.44 V vs. RHE in 1.0 M KOH with 30 mM furfural. (c) Yield curve of 2-furoic acid at 1.423 V vs. RHE in 1.0 M KOH with 30 mM furfural. (d) Ni 2p region for $Ni_2P$/Ni/NF after (red) and before (black) electrocatalytic furfural oxidation.

a much smaller potential. The catalytic onset cathodically shifted to 1.34 V vs. RHE, indicative of the more thermodynamically favorable oxidation of furfural to 2-furoic acid relative to water oxidation. Rapid catalytic current rise was obtained when scanning towards more positive potential. In fact, a current density of 200 mA cm$^{-2}$ was achieved at ≈1.41 V vs. RHE, nearly 180 mV smaller than that of pure water oxidation to reach the same current density. As demonstrated in Figure 2b, the current densities at 1.40, 1.42, and 1.44 V vs. RHE in the presence of furfural were at least 20 times larger than those in the absence of furfural.

In order to track the conversion of furfural and the yield of 2-furoic acid, a long-term chronoamperometry of furfural oxidation catalyzed by $Ni_2P$/Ni/NF was conducted at a constant potential of 1.423 V vs. RHE (Figure S4), as it was prior to the catalytic onset of water oxidation (Figures 2a). Since the oxidation of furfural to 2-furoic acid is a two-electron process, it was calculated that 116 C was required to transform 30 mM furfural (20 mL) completely to 2-furoic acid if a 100% Faradaic efficiency was assumed.

The concentration change of furfural and 2-furoic acid were quantified via high-performance liquid chromatography (HPLC) (Figure S5) according to pre-established calibration curves. As shown in Figure 2c, the concentration of furfural decreased along with the increasing concentration of 2-furoic acid as more charge was consumed over time, suggesting the continuous conversion of furfural into 2-furoic acid during the electrocatalytic process. After 116 C charge was consumed, nearly complete conversion of furfural (98%) was obtained with a 94% yield of 2-furoic acid.

The robustness of $Ni_2P$/Ni/NF was assessed by consecutive oxidation electrolysis with the same concentration of furfural (30 mM) in fresh 1.0 M KOH electrolyte and the same catalyst. The yields of 2-furoic acid of three continuous cycles were plotted in Figure S6, with all the yields falling in the range of 96% to 98%, demonstrating the remarkable stability of our $Ni_2P$/Ni/NF for furfural oxidation under alkaline condition.

Post-electrolysis analysis was also performed for $Ni_2P$/Ni/NF to shed light on its morphology and composition change. The low-magnification SEM image showed that the post-furfural-oxidation $Ni_2P$/Ni/NF inherited the overall 3D porous structure (Figure S7a). However, a close inspection of its high-magnification SEM images (Figure S7b–c) revealed the presence of featureless monoliths in addition to urchin-like microparticles, which was quite different from the fresh (Figure 1) and the post-HER samples (Figure S9). Elemental mapping results (Figure S7d) demonstrated that the post-furfural-oxidation $Ni_2P$/Ni/NF mainly consisted of Ni and P, plus a large concentration of O. Indeed, the high-resolution Ni 2p XPS spectrum of the post-furfural-oxidation $Ni_2P$/Ni/NF displayed a new peak at 858.8 eV (Figure 2d top), which could be attributed to nickel oxides formed during the electrocatalysis of furfural oxidation.

With the aforementioned results in hand, we are optimistic that $Ni_2P$/Ni/NF was able to catalyze both HER (Figure S8) and furfural oxidation simultaneously. Hence, a two-electrode electrolyzer employing $Ni_2P$/Ni/NF as both the anode and cathode catalysts was constructed. The two compartments of this electrolyzer were separated by an anion exchange membrane and 1.0 M KOH was used as the electrolyte. As a comparison, pure water splitting electrolysis was also assessed. In the absence of furfural in the anodic compartment, the $Ni_2P$/$Ni_2P$ couple was able to catalyze overall water splitting to produce $H_2$ and $O_2$ (Figure 3a). It required a voltage of 1.59 V to produce a catalytic current density of 10 mA cm$^{-2}$. In sharp contrast, upon addition of 30 mM furfural in the anodic compartment, the $Ni_2P$/Ni/NF catalyst couple exhibited a catalytic current at an onset potential less than 1.4 V (Figure 3a). Only 1.48 V was required to achieve the current density of 10 mA cm$^{-2}$, 110 mV smaller than that of sole water splitting. Figure 3b compares the produced catalytic current densities of our $Ni_2P$/Ni/NF catalyst couple in the presence and absence of furfural at three different voltages, 1.50, 1.55, and 1.60 V. The integrated HER and furfural oxidation system shows substantially higher catalytic current densities relative to those of only water splitting electrolysis, highlighting the improved return of voltage input of the former electrocatalytic coupling strategy.

Furthermore, the robustness of the $Ni_2P$/Ni/NF catalyst couple for this integrated electrolysis was evaluated by five successive electrolysis cycles using the same catalyst couple and fresh 1.0 M KOH electrolyte containing 30 mM furfural for each cycle. As plotted in Figure 3c, the yields of 2-furoic acid were maintained in the range of 97–99%, suggesting the

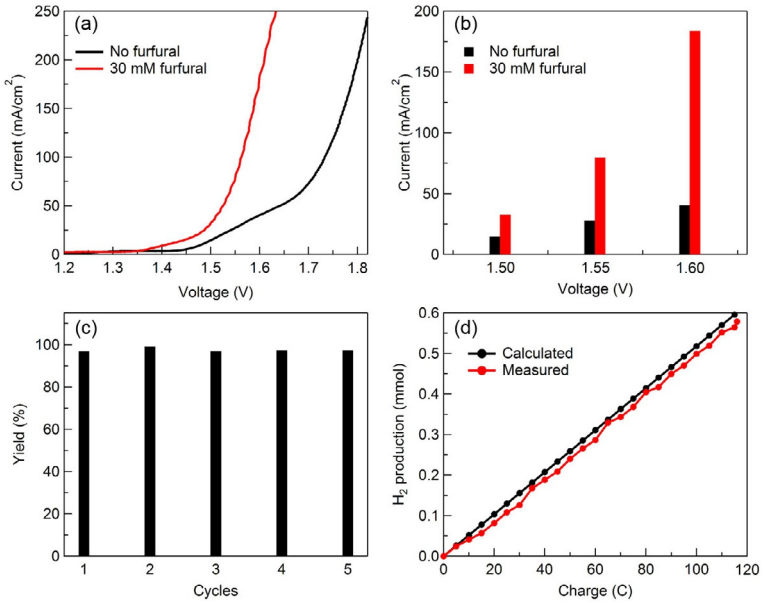


**Figure 3.** (a) LSV curves of $Ni_2P$/Ni/NF couple with (red) and without (black) 30 mM furfural in 1.0 M KOH. (b) Comparison of the current densities of $Ni_2P$/Ni/NF couple at 1.50, 1.55, and 1.60 V vs. RHE in 1.0 M KOH with (red) and without (black) 30 mM furfural. (c) Yield of 2-furoic acid catalyzed by the same $Ni_2P$/Ni/NF catalyst couple in 1.0 M KOH for five successive electrolysis cycles with 30 mM furfural for each cycle. (d) GC-measured $H_2$ quantity (red) compared with the calculated $H_2$ quantity (black) based on passed charge during the electrocatalysis with a $Ni_2P$/Ni/NF catalyst couple in 1.0 M KOH solution.

strong robustness of the $Ni_2P$/Ni/NF catalyst couple for this integrated electrolysis. In addition, nearly unity Faradaic efficiency was also obtained for the cathodic $H_2$ evolution reaction (Figure 3 d), as confirmed by the near overlap of gas-chromatography-measured $H_2$ quantity and the calculated amount based on passed charge during electrolysis (Figure S10). Post-electrolysis analysis was also carried out on the $N_2P$/Ni/NF catalyst couple. Figure S11 and S12 present the SEM and elemental mapping results of $Ni_2P$/Ni/NF as cathode and anode electrocatalysts, respectively, displaying similar results as those observed for the corresponding half reactions discussed previously.

## Conclusions

In summary, we have demonstrated a highly efficient electrochemical process employing $Ni_2P$/Ni/NF as a bifunctional electrocatalyst for the integrated $H_2$ production and furfural oxidation to 2-furoic acid. $Ni_2P$/Ni/NF solely consists of earth-abundant elements and it can be synthesized in a facile manner, suggesting its low cost for large-scale manufacture. When acting as the electrocatalysts for both cathode and anode, $Ni_2P$/Ni/NF demonstrated excellent reactivity, strong robustness, and nearly unity Faradaic efficiencies for both $H_2$ production and 2-furoic acid formation. High current density (i.e., 250 mA cm$^{-2}$) can be achieved at applied voltages much smaller than that of pure water splitting, manifesting its enhanced energy conversion efficiency. In addition, since furfural oxidation is only one of many potential organic oxidation reactions, we envision such an integrated strategy of $H_2$ production and organic oxidation will be able to be applied to a wide variety of organic transformations, resulting in numerous value-added products at the anode, instead of $O_2$.

## Experimental Section

**Chemicals:** Nickel chloride hexahydrate ($NiCl_2{\cdot}6H_2O$), ammonium chloride ($NH_4Cl$), sodium hypophosphite monohydrate ($NaH_2PO_2{\cdot}H_2O$), and potassium hydroxide (KOH) were all purchased from commercial vendors and used directly without any further purification. Furfural and 2-furoic acid were purchased from Tokyo Chemical Industry and Acros, respectively, and used as received. Nickel foam with purity >99.99% was purchased from MTI. Water was deionized (18 Ω·cm) using a Barnstead E-Pure system.

**Synthesis of Ni/NF:** The preparation of Ni/NF was conducted via chronopotentiometry according to our reported method.[14] Prior to electrodeposition, Ni foam was sonicated in 1.0 M HCl for 10 min to remove residual organic species. Typically, the electrodeposition of 3D porous Ni nanoparticles on nickel foam (Ni/NF) was performed in a standard two-electrode system at room temperature with an electrolyte consisting of 2.0 M $NH_4Cl$ and 0.1 M $NiCl_2$. A piece of nickel foam with a size of 0.5 cm × 1 cm was used as the working electrode and a Pt wire as the counter electrode. The electrodeposition was carried out at a constant current of −1.0 A cm$^{-2}$ for 500 s to obtain Ni/NF samples.

**Synthesis of $Ni_2P$/Ni/NF:** The resulting Ni/NF was placed at the center of a tube furnace, and 1.0 g $NaH_2PO_2{\cdot}H_2O$ was placed at the upstream side and near Ni/NF. After flushed with Ar for ≈20 min, the center of the furnace was quickly elevated to the reaction temperature of 400 °C with a ramping rate of 10 °C min$^{-1}$ and kept at 400 °C for 2 h to convert the metallic nickel to nickel phosphides.

**Physical Methods:** Scanning electron microscopy (SEM) and elemental mapping measurements were conducted on a FEI QUANTA FEG 650 (FEI, USA). X-ray diffraction (XRD) data were collected on a Rigaku MinifexII Desktop X-ray diffractometer. X-ray photoelectron spectra were recorded on a Kratos Axis Ultra instrument (Chestnut Ridge, NY). The samples were affixed on a stainless steel Kratos sample bar, loaded into the instrument's load lock chamber, and evacuated to $5\times10^{-8}$ torr before they were transferred into the sample analysis chamber under ultrahigh vacuum conditions

($\approx 10^{-10}$ torr). X-ray photoelectron spectra were collected using the monochromatic $Al_{K\alpha}$ source (1486.7 eV) at a 300×700 μm spot size. High resolution regions at the binding energy of interest were taken for each sample. The samples were also sputter cleaned inside the analysis chamber with 1 keV $Ar^+$ ions for 30 s to remove adventitious contaminants. The XPS data were analyzed using CASA XPS software and the energy corrections for high resolution spectra were calibrated by referencing the C 1s peak of adventitious carbon to 284.5 eV.

**Electrocatalytic Measurements:** Electrochemical experiments were performed on a computer-controlled Gamry Interface 1000 electrochemical workstation with a three-electrode configuration. Aqueous Ag/AgCl reference electrodes (saturated KCl) were purchased from CH Instruments. The reference electrode in aqueous media was calibrated with ferrocenecarboxylic acid whose $Fe^{3+/2+}$ couple is 0.284 V vs. SCE. All potentials reported in this paper were converted from vs. Ag/AgCl to vs. RHE (reversible hydrogen electrode) by adding a value of 0.197 + 0.059×pH. iR (current times internal resistance) compensation was applied in polarization and controlled potential electrolysis experiments to account for the voltage drop between the reference and working electrodes using the Gamary Framework™ Data Acquisition Software 6.11. The catalyst-coated NF was directly used as the working electrode. A Pt wire was used as the counter electrode. All the electrochemical measurements were conducted in 1.0 M KOH with a two-compartment cell in which the anode and cathode compartments were separated by an anion exchange membrane (Fumasep FAA-3-PK-130) purchased from Fuel Cell Store.

**Quantitative Product Analysis:** In order to analyze the product and furfural oxidation quantitatively, 100 μL of the electrolyte solution was periodically collected from the electrolyte solution during chronoamperometry and diluted with 900 μL water. Subsequently, the aforementioned solutions were further diluted 3 times with water. The final samples were then analyzed by HPLC (Shimadzu Prominence LC-2030C system) at room temperature to calculate the furfural conversion and the quantity of 2-furoic acid. The HPLC instrument was equipped with an ultraviolet-visible detector set at 265 nm and a 4.6 mm×150 mm Shim-pack GWS 5 μm C18 column. The eluent solvent is a mixture of 5 mM ammonium formate aqueous solution and methanol. Separation was accomplished using an isocratic elution by using 50% ammonium formate aqueous solution and 50% methanol for 10 min with the flow rate set at 0.5 mL $min^{-1}$. The quantification of furfural and its oxidation product was calculated based on the calibration curves of those standard compounds with known concentrations.

## Acknowledgements

We acknowledge the support of the National Science Foundation (CHE-1653978) and the Microscopy Core Facility at Utah State University. X.L. acknowledges the financial support from the Chinese Academy of Sciences Funded Overseas Study Program and Qinghai Institute of Salt Lakes, Chinese Academy of Sciences.

**Keywords:** biomass upgrading · electrocatalysis · furfural oxidation · hydrogen evolution · water splitting

[1] S. Chu, A. Majumdar, *Nature* **2012**, *488*, 294–303.
[2] a) J. A. Turner, *Science* **2004**, *305*, 972–974; b) D. G. Nocera, *Chem. Soc. Rev.* **2009**, *38*, 13–15; c) T. R. Cook, D. K. Dogutan, S. Y. Reece, Y. Surendranath, T. S. Teets, D. G. Nocera, *Chem. Rev.* **2010**, *110*, 6474–6502; d) R. E. Blankenship, D. M. Tiede, J. Barber, G. W. Brudvig, G. Fleming, M. Ghirardi, M. R. Gunner, W. Junge, D. M. Kramer, A. Melis, T. A. Moore, C. C. Moser, D. G. Nocera, A. J. Nozik, D. R. Ort, W. W. Parson, R. C. Prince, R. T. Sayre, *Science* **2011**, *332*, 805–809; e) H. B. Gray, *Nat. Chem.* **2009**, *1*, 7.
[3] N. S. Lewis, D. G. Nocera, *Proc. Natl. Acad. Sci. USA* **2006**, *103*, 15729–15735.
[4] A. Corma, S. Iborra, A. Velty, *Chem. Rev.* **2007**, *107*, 2411–2502.
[5] a) J. Cui, J. Tan, T. Deng, X. Cui, Y. Zhu, Y. Li, *Green Chem.* **2016**, *18*, 1619–1624; b) Y. Nakagawa, H. Nakazawa, H. Watanabe, K. Tomishige, *ChemCatChem* **2012**, *4*, 1791–1797.
[6] a) R. Mariscal, P. Maireles-Torres, M. Ojeda, I. Sadaba, M. Lopez Granados, *Energy Environ. Sci.* **2016**, *9*, 1144–1189; b) X. Li, P. Jia, T. Wang, *ACS Catal.* **2016**, *6*, 7621–7640.
[7] a) R. Radhakrishnan, K. Kannan, S. Kumaravel, S. Thiripuranthagan, *RSC Adv.* **2016**, *6*, 45907–45922; b) Z. Li, S. Kelkar, C. H. Lam, K. Luczek, J. E. Jackson, D. J. Miller, C. M. Saffron, *Electrochim. Acta* **2012**, *64*, 87–93.
[8] A. Halasa, L. Lapinski, I. Reva, H. Rostkowska, R. Fausto, M. J. Nowak, *J. Phys. Chem. A* **2015**, *119*, 1037–1047.
[9] A. Escobar, Á. Sathicq, L. Pizzio, M. Blanco, G. Romanelli, *Process Saf. Environ.* **2015**, *98*, 176–186.
[10] a) B. Zhao, M. Chen, Q. Guo, Y. Fu, *Electrochim. Acta* **2014**, *135*, 139–146; b) M. Manzoli, F. Menegazzo, M. Signoretto, G. Cruciani, F. Pinna, *J. Catal.* **2015**, *330*, 465–473; c) P. Parpot, A. P. Bettencourt, G. Chamoulaud, K. B. Kokoh, E. M. Belgsir, *Electrochim. Acta* **2004**, *49*, 397–403.
[11] X. Xiang, B. Zhang, G. Ding, J. Cui, H. Zheng, Y. Zhu, *Catal. Commun.* **2016**, *86*, 41–45.
[12] a) Y. Sun, C. Liu, D. C. Grauer, J. Yano, J. R. Long, P. Yang, C. J. Chang, *J. Am. Chem. Soc.* **2013**, *135*, 17699–17702; b) N. Jiang, L. Bogoev, M. Popova, S. Gul, J. Yano, Y. Sun, *J. Mater. Chem. A* **2014**, *2*, 19407–19414; c) N. Jiang, B. You, M. Sheng, Y. Sun, *Angew. Chem. Int. Ed.* **2015**, *54*, 6251–6254; *Angew. Chem.* **2015**, *127*, 6349–6352; d) B. You, N. Jiang, M. Sheng, W. S. Drisdell, J. Yano, Y. Sun, *ACS Catal.* **2015**, *5*, 7068–7076; e) B. You, N. Jiang, M. Sheng, S. Gul, J. Yano, Y. Sun, *Chem. Mater.* **2015**, *27*, 7636–7642; f) B. You, N. Jiang, M. Sheng, Y. Sun, *Chem. Commun.* **2015**, *51*, 4252–4255; g) N. Jiang, Q. Tang, M. Sheng, B. You, D.-e. Jiang, Y. Sun, *Catal. Sci. Technol.* **2016**, *6*, 1077–1084; h) N. Jiang, B. You, M. Sheng, Y. Sun, *ChemCatChem* **2016**, *8*, 106–112; i) X. Liu, J. Dong, B. You, Y. Sun, *RSC Adv.* **2016**, *6*, 73336–73342; j) B. You, N. Jiang, Y. Sun, *Inorg. Chem. Front.* **2016**, *3*, 279–285; k) B. You, Y. Sun, *Adv. Energy Mater.* **2016**, *6*, 1502333; l) B. You, Y. Sun, *ChemPlusChem* **2016**, *81*, 1045–1055; m) Y. Shi, Y. Xu, S. Zhuo, J. Zhang, B. Zhang, *ACS Appl. Mater. Interfaces* **2015**, *7*, 2376–2384; n) C. Zhang, Y. Huang, Y. Yu, J. Zhang, S. Zhuo, B. Zhang, *Chem. Sci.* **2017**, *8*, 2769–2775; o) X. Wang, Y. V. Kolen'ko, L. Liu, *Chem. Commun.* **2015**, *51*, 6738–6741; p) X. Wang, Y. V. Kolen'ko, X. Bao, K. Kovnir, L. Liu, *Angew. Chem.* **2015**, *127*, 8306–8310; *Angew. Chem. Int. Ed.* **2015**, *54*, 8188–8192; q) X. Wang, W. Li, D. Xiong, D. Y. Petrovykh, L. Liu, *Adv. Funct. Mater.* **2016**, *26*, 4067–4077; r) W. Li, X. Gao, D. Xiong, F. Xia, J. Liu, W. Song, J. Xu, S. M. Thalluri, M. F. Cerqueira, X. Fue, L. Liu, *Chem. Sci.* **2017**, *8*, 2952–2958.
[13] a) B. You, N. Jiang, X. Liu, Y. Sun, *Angew. Chem. Int. Ed.* **2016**, *55*, 9913–9917; *Angew. Chem.* **2016**, *128*, 10067–10071; b) N. Jiang, B. You, R. Boonstra, I. M. Terrero Rodriguez, Y. Sun, *ACS Energy Lett.* **2016**, *1*, 386–390; c) B. You, X. Liu, N. Jiang, Y. Sun, *J. Am. Chem. Soc.* **2016**, *138*, 13639–13646.
[14] B. You, N. Jiang, M. Sheng, M. W. Bhushan, Y. Sun, *ACS Catal.* **2016**, *6*, 714–721.
[15] a) L.-A. Stern, L. Feng, F. Song, X. Hu, *Energy Environ. Sci.* **2015**, *8*, 2347–2351; b) Y. Pan, Y. Liu, J. Zhao, K. Yang, J. Liang, D. Liu, W. Hu, D. Liu, Y. Liu, C. Liu, *J. Mater. Chem. A* **2015**, *3*, 1656–1665.
[16] a) G. Grabowski, J. Lewkowski, R. Skowroński, *Electrochim. Acta* **1991**, *36*, 1995; b) K. R. Vuyyuru, P. Strasser, *Catal. Today* **2012**, *195*, 144–154; c) D. J. Chadderdon, L. Xin, J. Qi, Y. Qiu, P. Krishna, K. L. More, W. Li, *Green Chem.* **2014**, *16*, 3778–3786.
[17] W. T. Hong, M. Risch, K. A. Stoerzinger, A. Grimaud, J. Suntivich, Y. Shao-Horn, *Energy Environ. Sci.* **2015**, *8*, 1404–1427.

Manuscript received: March 20, 2017
Accepted manuscript online: April 9, 2017
Version of record online: May 3, 2017